Atomic Force Microscopy of Biological Samples

P.L.T.M. Frederix, B.W. Hoogenboom, D. Fotiadis, D.J. Müller, and A. Engel

Abstract

The atomic force microscope (AFM) allows biomolecules to be observed and manipulated under native conditions. It produces images with an outstanding signal-to-noise ratio and addresses single molecules while the sample is in a buffer solution. Progress in sample preparation and instrumentation has led to topographs that reveal subnanometer details and the surface dynamics of biomolecules. Tethering single molecules between a support and a retracting AFM tip produces force–extension curves, giving information about the mechanical stability of secondary structural elements. For both imaging and force spectroscopy, the cantilever and its tip are critical: the mechanical properties of the cantilever dictate the force sensitivity and the scanning speed, whereas the tip shape determines the achievable lateral resolution.

Keywords: *atomic force microscopy, biological molecules, imaging, native membranes, protein dynamics, single-molecule force spectroscopy.*

Introduction

The number of resolved three-dimensional (3D) structures of biological molecules and complexes imaged at atomic resolution is increasing every year. These structures are obtained from large ensembles of molecules in the same configuration. Occasionally, it has been possible to arrest biomolecules in different configurations and consequently resolve the structure of the different states. However, it is still difficult to assess the dynamic changes in these nanomachines during their functional cycles. In order for researchers to observe biomolecules at work, the biomolecules must reside in a physiological environment in which they can carry out their cycles. For soluble proteins, this is a physiological buffer, while membrane proteins also need to be embedded in a lipid bilayer. The atomic force microscope (AFM)[1] is still the only instrument that provides subnanometer spatial resolution and that can be operated with the sample in solution. This makes it an important characterization tool for biological samples, despite the limitation that it can only provide information on the structure and dynamics of the sample surface. Progress has been achieved by optimizing sample preparation[2–5] and image acquisition methods[6,7] and by continuous development of the instrumentation[8–11] (see sidebar article).

Topographs of the surfaces of biomolecules acquired by AFM reveal the objects in their most native state. The high signal-to-noise ratio provided by this technique allows submolecular features to be discerned on single biomolecules. Moreover, structural variations at their surfaces can be detected that correspond to conformational changes of the molecule at work. In addition, the AFM stylus is a nanotool that allows single molecules to be manipulated—for example, biomolecules can be tethered between the stylus and the support and unfolded as the stylus-to-support distance is increased. The forces and associated distances measured during this process give novel information on the nature and position of molecular interactions and on the forces that stabilize the biomolecules in their configurations. In this review, we discuss the application of AFM as a tool for imaging and manipulating single molecules.

DLVO Forces

To achieve high resolution, topographs are recorded with the sample in a buffer solution. In this case, mainly electrostatic and van der Waals forces govern the tip–sample interactions. In biological systems measured in aqueous solution, van der Waals interactions do not depend on the ionic strength; they decay rapidly and are always attractive. Electrostatic interactions result from hydrophilic surfaces that are often charged in water. These interactions are long-range and can be attractive or repulsive, depending on the sign of the surface charges, which in turn depends on the pH. Since the Si_3N_4 stylus is negatively charged at neutral pH, and protein layers are often negatively charged as well, the electrostatic forces are in most instances repulsive. The surface charges can be screened with electrolytes, and the electrolyte concentration determines the decay of the electrostatic interactions. In this way, the interactions can be controlled.

The DLVO (Derjaguin, Landau, Verwey, and Overbeek) theory describes these forces quantitatively and allows the interactions between a spherical tip and a planar sample to be modeled, providing clues to optimizing the conditions.[6] At optimal conditions, the tip surfs on a cushion of electrostatic repulsion, while a small asperity on the tip contacts the sample without inducing deformation.[6] Figure 1 illustrates this situation, showing the changes in the repulsive electrostatic forces between the stylus and the sample resulting from changes in the ionic strength. If the ionic strength is too low (Figure 1b, top curve, 20 mM KCl), there is a large electrostatic repulsion before contact is achieved. If the ionic strength is too high (Figure 1b, bottom curve, 100 mM KCl with 50 mM $MgCl_2$), the electrostatic force has a shorter range than the van der Waals attraction, and the tip is pulled into the surface. In both cases, high-resolution topographs cannot be recorded at minimal force conditions.

Imaging

When operating commercial AFMs under optimal conditions, the surfaces of biomolecules can be contoured routinely at a lateral resolution of <1 nm and a vertical resolution of $\sim$0.1 nm.

Figure 2 shows an image of the extracellular surface of a purple membrane crystal, a natural two-dimensional (2D) crystal composed of bacteriorhodopsin (bR) trimers (see the outlined trimer unit in Figure 2a) and lipids.[12] The topograph shows the conformation of the extracellular surface of bR scanned in a physiological buffer solution. Structural details in the trimer can be clearly distinguished. The 2D power spectrum of this topograph (Figure 2b) gives a good indication of the resolution obtained in such an image. Many diffraction spots are visible

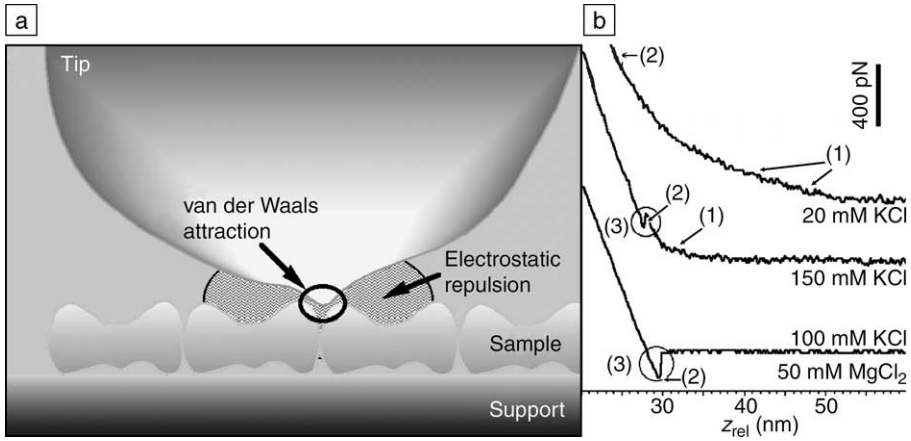

Figure 1. Tip–sample forces. (a) Schematic representation of the dominant forces on a tip in close proximity to a sample surface. (b) Force (y axis) versus distance (x axis) curves recorded on an extracellular purple membrane surface consisting of regularly packed bacteriorhodopsin (bR) trimers and lipid molecules. Data were obtained for different electrolyte concentrations at pH = 7.6. Force–distance curves were recorded during the approach of the sample and the AFM tip. Scan frequency, 1.97 Hz; scan range, 50 nm (512 pixels); the vertical bar denotes a force of 400 pN. Arrows labeled "(1)" mark the onset of measurable electrostatic repulsion, whereas arrows labeled "(2)" indicate the point of contact between tip and sample. At the circled areas labeled "(3)," the cantilever is pulled into the sample by the van der Waals force.

beyond $(1\ \text{nm})^{-1}$ (dashed semicircle) in the power spectrum, with spots corresponding to a real-space resolution of 0.46 nm (e.g., the diffraction spot circled in Figure 2b).[13]

Figure 3 shows the cytoplasmic surface of bR. The major protrusions are at the periphery of the trimers and protrude 0.8 nm out of the membrane. These protrusions reflect the E–F loop connecting transmembrane helices E and F (marked with a dashed ellipse in Figures 3b–d, see also Figure 5c).[14] Smaller protrusions reflect the shorter A–B loop connecting helices A and B (marked with a solid circle in Figures 3b–d). A third loop, connecting helices C and D, is hidden by the large E–F loop. To record this image, the force applied to the stylus was approximately 50 pN, preventing a force-induced conformational change of the E–F loop. This loop is known to deform when the force is increased to >100 pN, thereby changing the conformation of the bR surface.[15] Interestingly, observations of different atomic models from x-ray crystallography show that the variation of this region is pronounced: the E–F loop is involved in the contacts leading to the 3D crystals, and its conformation is dictated by the 3D packing arrangement of the bR molecules. Although all the bR trimers are identical in the 2D crystal displayed in Figure 3a, their surface structure varies significantly. These changes are related to the flexibility of the bR surface rather than any noise introduced by the AFM. The flexibility of the surface lowers the resolution of the ensemble, but structural details of each trimer are still discernable. The variations in the trimer structure can be used to calculate the probability of finding a certain loop at a certain position (x,y) by mapping the corresponding peak positions of all individual bR trimers.[16] The E–F loop, which exhibits significant flexibility, is more delocalized than the A–B loop, which occupies a more defined position. The signal about the threefold axis results from a lipid molecule protruding 0.1 nm, which is only occasionally visible in the raw data, but if present, is precisely localized in the center of the trimer. Therefore, a strong signal emerges in the probability map (Figure 3c), whereas no signal is present in the average (Figure 3b). Precise localization of a surface feature suggests that the corresponding

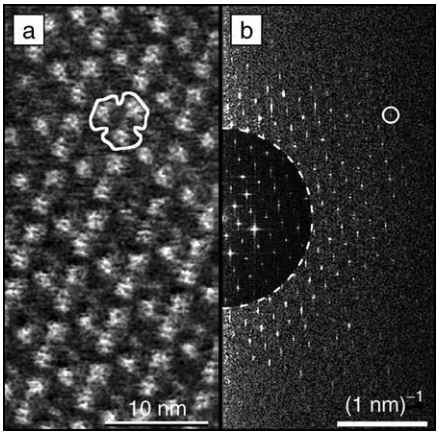

Figure 2. Atomic force microscope imaging at high resolution. (a) The extracellular surface of a purple membrane crystal, which consists of regularly packed bacteriorhodopsin (bR) trimers (one trimer is outlined in white) and lipid molecules. The height represented by the lightest areas of the gray scale is 0.8 nm. (b) The corresponding two-dimensional power spectrum in reciprocal space. The dashed half-circle is at $(1\ \text{nm})^{-1}$, and the small circle marks a diffraction spot at $(0.46\ \text{nm})^{-1}$.

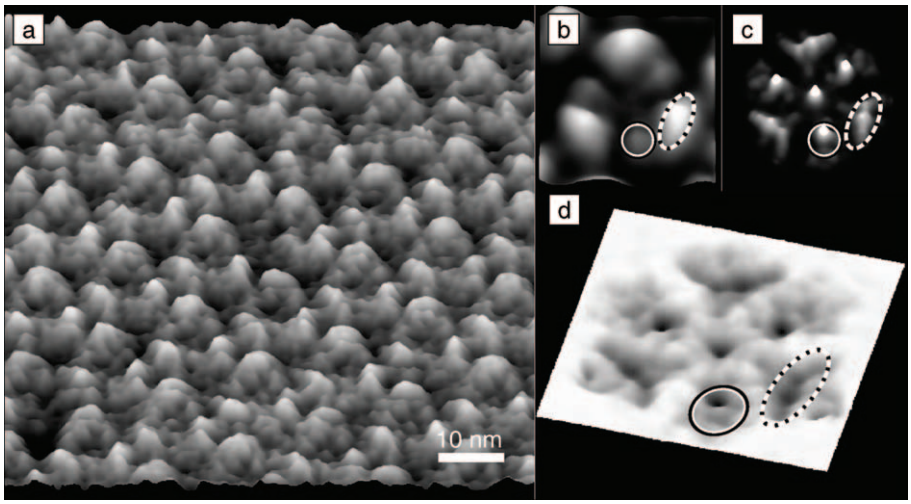

Figure 3. Atomic force microscope image of protein dynamics. (a) Cytoplasmic surface of a purple membrane crystal. The height represented by the lightest areas of the gray scale is 0.8 nm. (b) Average configuration of 1403 trimers. (c) Probability map showing the probability p to find a maximum at a given position (x,y). (d) The corresponding energy landscape. (b)–(d) have frame sizes of 7.7 nm, and the energy in (d) represented by the full gray scale is $\Delta E = 4.5$kT. See text for details.

structure is stabilized in a deeper potential well than a floppy feature, which may exhibit pronounced thermal motion. The position probability map $p(x,y)$ is readily converted to a free-energy landscape G using Boltzmann's law:

$$G(x,y) = -k_B T \ln[p(x,y)], \quad (1)$$

where k_B is the Boltzmann constant and T is the absolute temperature. The energy landscape of the cytoplasmic side of bR is shown in Figure 3d. This information relies on the capability of AFM to address individual molecules with sufficiently high resolution and signal-to-noise ratio.

To learn more about the structure and functioning of membrane proteins, it is important to study them in their functional form. This is best achieved by studying the proteins under native or near-native biological conditions (ideally, in their native membranes). The AFM is currently the only instrument that allows imaging under these conditions in combination with a resolution of <2 nm. Recently, AFM images of the disc membranes of rodent retinas have elucidated the arrangement of rhodopsin molecules that pack in rows of dimers[17] (Figure 4), in contrast to early optical studies.

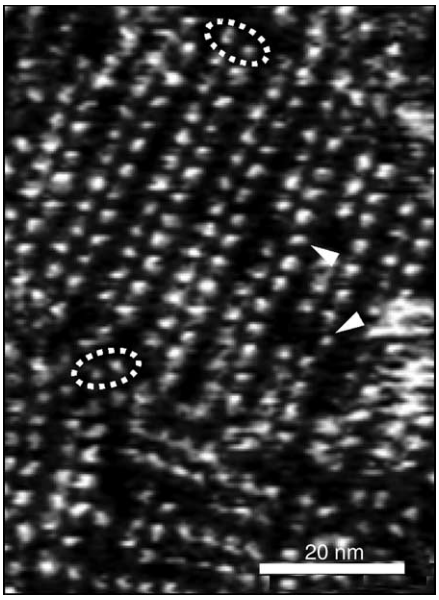

Figure 4. Atomic force microscope imaging of native membranes: paracrystalline organization of rhodopsin in native disc membranes of rodent retinas. Most of the rhodopsin molecules are present in dimers (see areas marked by dotted ellipses), although monomers are occasionally observed as well (indicated by arrowheads). The height represented by the lightest areas of the gray scale is 1.6 nm.

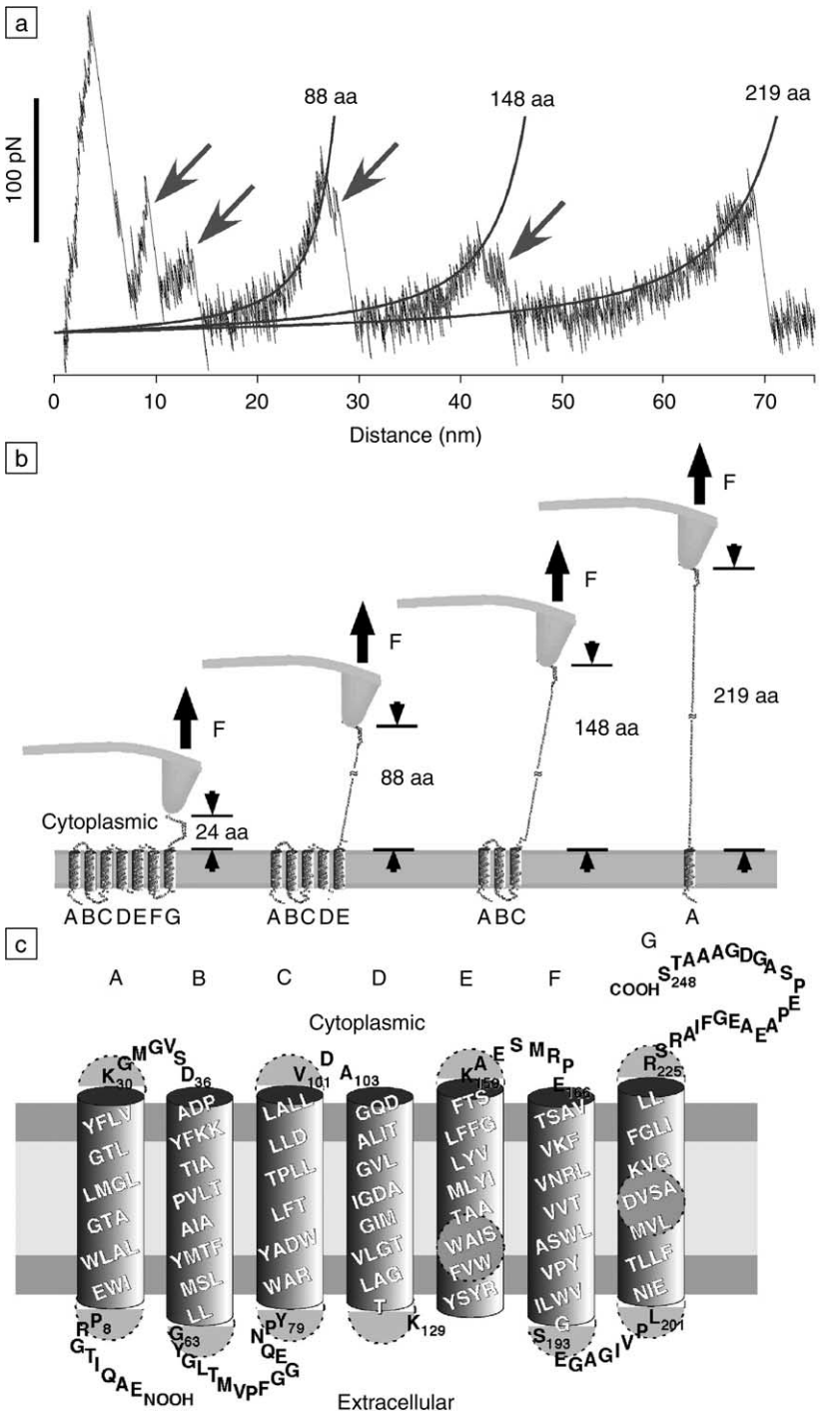

Figure 5. Assessing topology and the secondary structure of membrane proteins by single-molecule force spectroscopy. (a) Typical force–extension curve recorded while unfolding an individual bR molecule from native purple membrane. The force curve can be divided into major peaks (with fitted curves) and minor peaks (arrows). The fitted lengths of the major peaks, expressed in number of amino acids (aa), are given above the curves. (b) Schematic illustration of the origin of the major peaks as the pairwise unfolding of transmembrane α-helices. (c) Sequence of bR in one-letter symbols of the amino acids. The full and half-circles represent stabilizing amino acids derived from the fitted lengths (in aa units, counted from the C-terminus, COOH) of major and minor peaks in force–extension curves. By counting the aa units in each schematic in (b) from the aa number of the C-terminus in (c), 248, the aa positions marked by the four half-circles at the tops of the cylinders in (c) are obtained.

In addition, topographs of the native photosynthetic membrane of *Rhodopseudomonas viridis* bacteria have revealed the molecular organization of the photosynthetic core complex.[18]

The examples shown were recorded at minimal forces (<100 pN) to prevent deformation of the molecules, which would cause a reduction in resolution. However, at higher forces, the stylus may be used as a nanoscalpel to disrupt supramolecular assemblies.[19] In this case, the force applied to the tip is increased to 0.75–10 nN, depending on the desired level of disruption. Quite small forces (typically 1 nN) are sufficient to separate stacked layers of membranes or 2D crystals.[20–22] Even smaller forces and repeated scanning at high magnification suffice to push away extrinsic proteins that are specifically complexed to an integral membrane protein.[18,23–25]

Atomic Force Microscopy: Instrumentation Overview

Process and Experimental Setup

In atomic force microscopy (AFM), a map of the surface topography of a material is recorded by raster-scanning a sample below the tip, or stylus, of a probe attached to a flexible cantilever within the microscope. The tip follows the contours of the sample, and with an optical system, the deflection of the cantilever can be resolved to better than 0.1 nm accuracy.

In contact-mode imaging (see Figure), the deflection signal is coupled to a feedback loop that displaces the sample or the cantilever vertically in order to maintain a constant cantilever deflection. With modern instruments and an appropriate cantilever, stable contact-mode imaging is possible at forces of about 50 pN, provided that the sample is in an aqueous solution.

Alternatively, it is possible to oscillate the cantilever during scanning, intermittently touching the sample. The cyclic contact reduces the amplitude of the oscillation and gives a phase shift. Using the oscillation amplitude for feedback (Figure, b) allows scanning at a lower lateral force than in contact-mode imaging, which is particularly interesting for the study of single particles. By measuring the oscillation phase (Figure, c), information on the sample stiffness can be acquired.

The experimental setup of an atomic force microscope is shown in (d), which allows scanning of a sample in a buffer solution. With a typical cantilever (Figure, e), forces from slightly less than 50 pN to 2000 pN can be measured. Tethering biomolecules between the support and the tip allows the recording of force–distance spectra as the tip–support distance is increased. To record such force–distance curves, the tip approaches the sample vertically and is then retracted until a molecule has attached to it. In the case of crystalline protein layers such as protein-packed membranes or bacterial surface layers, biomolecules can be removed from the layer ("unzipping" them).[1] Acquisition of high-resolution images before and after the unzipping of a biomolecule allows the result of the unzipping event (a hole) to be directly visualized.

Cantilevers and Tips: Parameters and Optimization

Cantilevers for AFM are produced by microfabrication. The geometry (shape, length l, width w, and thickness t), density (ρ), and elasticity modulus (E) dictate the mechanical properties of a cantilever, generally expressed by the spring constant (k_L) and the resonance frequency (f_0) in vacuum:

$$k_L = \left(\frac{1}{4}\right)\left(\frac{Ewt^3}{l^3}\right) \quad (1)$$

and

$$f_0 = \frac{ct\sqrt{E/\rho}}{l^2}. \quad (2)$$

Here, c is a shape-dependent constant that amounts to $c = 0.164$ for a rectangular cantilever. For imaging biological samples in contact mode, the spring constant of the cantilever should be taken as between 0.01 N/m and 0.1 N/m. The resonance frequency for these cantilevers ranges from 5 kHz to 50 kHz in vacuum and is slightly lower in air. When operating the cantilever in an aqueous solution, the resonance frequency is reduced by a factor of 2–5. For example, a conventional rectangular silicon nitride cantilever (E = 129 GPa, ρ = 3440 kg/m^3)[2] with l = 100 μm, w = 40 μm, and t = 0.4 μm has a spring constant of $k_L = 0.08$ N/m and a resonance frequency in vacuum of f_0 = 40 kHz.

Another parameter characterizing the cantilever is the quality factor Q, which is defined by the stored energy W_0 and the total energy loss per oscillation cycle ΔW:[2]

$$Q = 2\pi W_0/\Delta W. \quad (3)$$

In high vacuum, Q is a true cantilever parameter because the energy losses result from internal damping mechanisms.[2,3] However, in air or in fluid, hydrodynamic damping by the surrounding medium dominates the energy losses.[2–4] While suitable contact-mode cantilevers have a quality factor of Q = 10–100 in air, typical values drop down to Q = 1–5 when the cantilevers are operated in fluid.

The resonance frequency and quality factor can be determined from the noise in the deflection signal,[5] even when no oscillation mode is available. The thermal noise spectrum of the cantilever in water or air can be obtained by recording the deflection signal without a sample in close proximity and at a sampling rate that is at least twice the resonance frequency of the cantilever.

The k_L value can be calculated from the amplitude (in nm) of the thermal deflection noise, using the fluctuation method.[6] To obtain this amplitude, the deflection signal (usually a voltage) needs to be calibrated. Alternatively, the spring constant can be derived from the f_0 and Q values of the cantilever, together with its top-view dimensions.[7] Calibration of the deflection signal is not required in this case. The method assumes that the energy losses are dominated by the hydrodynamic damping, implying that the density and viscosity of the surrounding medium (air or liquid) are known. This method[7] was derived for rectangular cantilevers, but can be extended to different shapes as well if a reference cantilever is available.[7,8] Both methods[6,7] give an uncertainty of <20%.

The minimum force (F_{min}) that a cantilever can measure is ultimately limited by the thermal noise of the cantilever. This can be expressed as a function of the spring constant, resonance frequency, and quality factor, or in the case of vacuum, as a function of the dimensions of the cantilever and the quality factor:

Single-Molecule Force Spectroscopy

Tethering single biological molecules between an AFM tip and the supporting surface allows the force–distance relationship of a protein to be measured. This approach was used to characterize forces that mediate molecular recognition as well as to demonstrate the correlation between folding patterns and unfolding forces.[26–33] Models such as the worm-like chain (WLC) model, which were originally developed to describe the molecular compliance of polymers, were applied to the discrete unfolding events of single proteins to give information on chain lengths and disruption forces. Such forced unfolding experiments performed on water-soluble proteins such as fibronectin and titin[26,28,31] showed that these proteins unfold in an all-or-nothing event with no intermediate states. In rare

$$F_{\min} = \sqrt{\left(\frac{4k_BTB}{2\pi}\right)\left(\frac{k_L}{f_0Q}\right)} = \sqrt{\left(\frac{k_BTB}{2\pi}\right)\left(\frac{wt^2}{lQc}\right)}\sqrt[4]{E\rho}, \qquad (4)$$

where k_B is the Boltzmann constant, T is the absolute temperature, and B is the measurement bandwidth.[2] For a cantilever with $k_L = 0.08$ N/m and assuming $f_0 = 10$ kHz and $Q = 2$ in fluid, operated at room temperature with a sampling rate equal to the resonance frequency (i.e., $B = 10$ kHz), Equation 4 gives a minimal detectable force of about 10 pN.

This equation helps to optimize cantilever dimensions to achieve high force sensitivity within the boundary conditions determined by k_L (0.01–0.1 N/m) and the limitations of microfabrication. In addition, a high f_0 value is desirable, to allow high recording speeds for observing real-time dynamics.

Both goals—a better force sensitivity and a higher measurement speed—can be achieved by reducing the cantilever dimensions. For example, a 20-μm-long rectangular cantilever with $w = 5$ μm and $t = 0.16$ μm has a 10× higher resonance frequency in vacuum than the conventional 100-μm-long rectangular cantilever mentioned earlier, while exhibiting the same k_L value (0.08 N/m). Thus, in contact mode, the sensitivity of the smaller cantilever is enhanced by a factor of three when operated at the same bandwidth as a conventional cantilever. Alternatively, the measurement speed can be increased by a factor of 10 without an increase in the thermal noise.

Another parameter of the cantilever is tip sharpness. Although suppliers specify tip radii of no better than 10–50 nm, topographs of flat biological surfaces with a resolution of better than 1 nm have been routinely acquired.[9–12] Provided that long-range interactions (e.g., electrostatic forces) are compensated for, only the short-range forces determine the tip–sample interaction. Consequently, only the tip atoms nearest the sample determine the lateral resolution, which is considerably smaller than would be expected based on the tip radius only. The tips employed in the high-resolution (1 nm or better) topographs most likely had a small asperity that protruded sufficiently to contour the finest surface structures. Such a small asperity can exert a prohibitively high pressure on the underlying structure, inducing its deformation. However, as explained in the main article, electrolytes can be used to adjust the tip–sample interactions, provided that the electrostatic forces are repulsive.

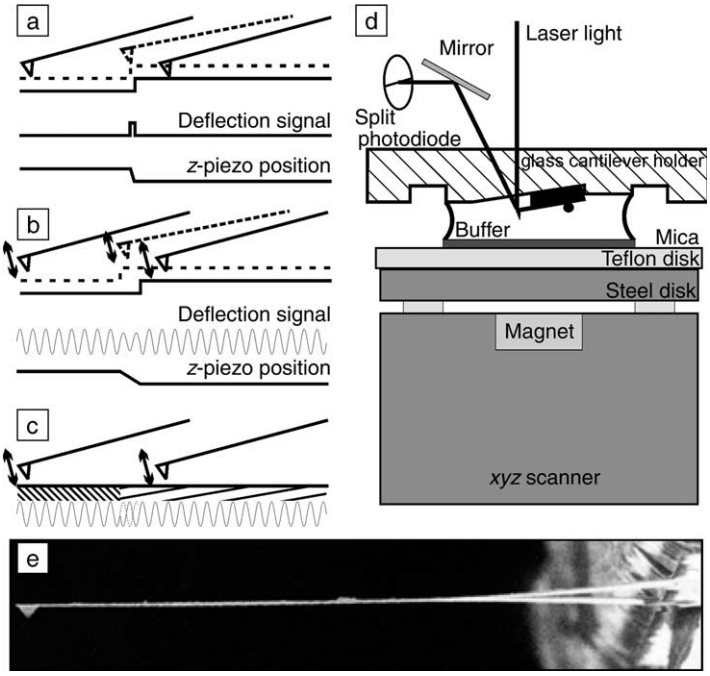

Figure. Atomic force microscopy (AFM) operation modes and instrumentation. (a) Contact mode, using the cantilever deflection as feedback signal. (b) Oscillation mode, using the oscillation amplitude as a feedback signal. (c) Oscillation mode, monitoring the phase difference between the driving force and cantilever oscillation. (d) Experimental setup for an atomic force microscope. A computer is used to control the movements of the sample and cantilever and store data on the surface contours measured. The instrument is operated with the sample adsorbed on a solid support (e.g., mica) in a buffer solution under ambient conditions. (e) Scanning electron microscopy image of an AFM cantilever and pyramidal tip. The contact-mode cantilever used for biological applications is a rectangular or triangular blade, typically ~0.4–0.8 μm thick, 100–200 μm long, and 20–40 μm wide. The pyramidal tip has a spherical end with a radius as small as 10 nm.

References

1. D.J. Müller, W. Baumeister, and A. Engel, *Proc. Natl. Acad. Sci.* U.S.A. **96** (1999) p. 13170.
2. K.Y. Yasumura, T.D. Stowe, E.M. Chow, T. Pfafman, T.W. Kenny, B.C. Stipe, and D. Rugar, *J. Microelectromech. Syst.* **9** (2000) p. 117.
3. J. Yang, T. Ono, and M. Esashi, *J. Microelectromech. Syst.* **11** (2002) p. 775.
4. J.E. Sader, *J. Appl. Phys.* **84** (1998) p. 64.
5. J.W.M. Chon, P. Mulvaney, and J.E. Sader, *J. Appl. Phys.* **87** (2000) p. 3978.
6. J.L. Hutter and J. Bechhöfer, *Rev. Sci. Instrum.* **64** (1993) p. 3342.
7. J.E. Sader, J.W.M. Chon, and P. Mulvaney, *Rev. Sci. Instrum.* **70** (1999) p. 3967.
8. C.T. Gibson, D.J. Johnson, C. Anderson, C. Abell, and T. Rayment, *Rev. Sci. Instrum.* **75** (2004) p. 565.
9. D.M. Czajkowsky, S. Sheng, and Z. Shao, *J. Mol. Biol.* **276** (1998) p. 325.
10. A. Engel and D.J. Müller, *Nat. Struct. Biol.* **7** (2000) p. 715.
11. D.J. Müller and A. Engel, *J. Mol. Biol.* **285** (1999) p. 1347.
12. F.A. Schabert, C. Henn, and A. Engel, *Science* **268** (1995) p. 92. □

cases, however, intermittent unfolding steps could be detected in titin.[34]

Force spectroscopy has been extended to proteins that are embedded in 2D layers. The combination of single-molecule imaging and force spectroscopy allows individual proteins to be manipulated in a controlled manner and molecular interactions to be measured.[19] This method provides a surprisingly detailed insight into forces that stabilize the protein fold in the layer.[35,36] Statistical analysis of unfolding spectra of bR[36] (see Figure 5) or of human aquaporin-1[37] (a cell membrane water channel) revealed that single membrane proteins choose individual but highly reproducible unfolding pathways, showing intermediate states related to their secondary structures. Individual potential barriers in the protein sequence (full- and half-circle areas in Figure 5c) were determined from chain length fits. Each potential barrier exhibits a specific probability of appearing in the unfolding pathway. Accordingly, unfolding of both individual and pairs of transmembrane helical segments are possible for these two membrane proteins. Most surprisingly, the probability for a particular unfolding pathway depends on local changes in the protein structure[36] and on the environment.[38]

Perspectives

Progress in instrumentation and sample preparation methods have opened avenues to image, manipulate, and assess the nanomechanics of single molecules. Such novel experimental possibilities find a wide range of applications in the study of the structure and function of biomolecules, the building blocks of life. While the large signal-to-noise ratio and resolution of the atomic force microscope allows the conformational states of single-protein surfaces to be probed at a lateral and vertical resolution of 0.4–1 nm and 0.1–0.2 nm, respectively, the force sensitivity (>20 pN) of this instrument also opens the door to measure the forces required to unfold a single protein. An unprecedented insight into the nature of intra- and intermolecular interactions in and between biomolecules is achieved by combining single-molecule imaging and force spectroscopy.

To enable real-time recording of the conformational changes of biomolecules during their functional cycles, further progress in instrumentation is required to increase the measurement speed. This progress includes the development of faster scanners,[39] smaller cantilevers,[40–42] and new deflection sensors that are capable of handling the minute cantilevers at high speed.[10,42–44]

These instrumental developments—for example, smaller cantilevers and better deflection sensors—will also further reduce the detection noise, allowing imaging at lower resolution, better-resolved forces, and force spectroscopy with improved force resolution (again, see the sidebar on instrumentation).

Another instrumental development is in the area of multifunctional cantilevers. Here, the aim is the design of cantilevers that combine the high spatial resolution of the AFM with the capability of applying local stimuli to the sample or to locally detect additional signals. The most straightforward example is a cantilever that is electrically conductive.[45,46] Such cantilevers enable the study of conformational changes in proteins as a function of the applied voltage between the cantilever tip and the support. This could, for example, help researchers to better understand the opening/closing mechanism of ion channels. In addition, electron tunneling through reaction-center complexes can be studied. Other types of multifunctional cantilevers include ones that can locally deliver light (i.e., cantilevered scanning near-field optical microscopy probes)[47,48] or ions (i.e., cantilevered pipettes).[49,50] The limitation and big challenge in the design of all of these cantilevers are that the spring constant, resonance frequency, and tip quality should be comparable to those of conventional cantilevers that are currently used for imaging in order to maintain the high spatial resolution in combination with the added functionality.

Acknowledgments

The research reviewed here was in part supported by the Swiss National Research Foundation (TOP NANO21 program), the Swiss National Centers for Competence in Research in Nanoscale Sciences and in Structural Biology, and the M.E. Müller Foundation.

References

1. G. Binnig, C.F. Quate, and C. Gerber, *Phys. Rev. Lett*. **56** (1986) p. 930.
2. J. Mou, J. Yang, and Z. Shao, *J. Mol. Biol.* **248** (1995) p. 507.
3. D.J. Müller, M. Amrein, and A. Engel, *J. Struct. Biol.* **119** (1997) p. 172.
4. D.M. Czajkowsky, S. Sheng, and Z. Shao, *J. Mol. Biol.* **276** (1998) p. 325.
5. S. Scheuring, F. Reiss-Husson, A. Engel, J.L. Rigaud, and J.L. Ranck, *EMBO J*. **20** (2001) p. 3029.
6. D.J. Müller, D. Fotiadis, S. Scheuring, S.A. Müller, and A. Engel, *Biophys. J*. **76** (1999) p. 1101.
7. C. Möller, M. Allen, V. Elings, A. Engel, and D.J. Müller, *Biophys. J.* **77** (1999) p. 1150.
8. P.K. Hansma, J.P. Cleveland, M. Radmacher, D.A. Walters, P.E. Hillner, M. Bezanilla, M. Fritz, D. Vie, H.G. Hansma, C.B. Prater, J. Massie, L. Fukunaga, J. Gurley, and V. Elings, *Appl. Phys. Lett.* **64** (1994) p. 1738.
9. W. Han, S.M. Lindsay, M. Dlakic, and R.E. Harrington, *Nature* **386** (1997) p. 563.
10. M.B. Viani, T.E. Schäffer, G.T. Paloczi, L.I. Pietrasanta, B.L. Smith, J.B. Thompson, M. Richter, M. Rief, H.E. Gaub, K.W. Plaxco, A.N. Cleland, H.G. Hansma, and P.K. Hansma, *Rev. Sci. Instrum.* **70** (1999) p. 4300.
11. A. Grant and L. McDonnell, *Ultramicroscopy* **97** (2003) p. 177.
12. A.E. Blaurock and W. Stoeckenius, *Nature New Biol.* **233** (1971) p. 152.
13. D. Fotiadis and A. Engel, *Methods Mol. Biol.* **242** (2004) p. 291.
14. D.J. Müller, J.B. Heymann, F. Oesterhelt, C. Möller, H. Gaub, G. Büldt, and A. Engel, *Biochim. Biophys. Acta* **1460** (2000) p. 27.
15. D.J. Müller, G. Büldt, and A. Engel, *J. Mol. Biol.* **249** (1995) p. 239.
16. S. Scheuring, D.J. Müller, H. Stahlberg, H.A. Engel, and A. Engel, *Eur. Biophys. J.* **31** (2002) p. 172.
17. D. Fotiadis, Y. Liang, S. Filipek, D.A. Saperstein, A. Engel, and K. Palczewski, *Nature* **421** (2003) p. 127.
18. S. Scheuring, J. Seguin, S. Marco, D. Levy, B. Robert, and J.L. Rigaud, *Proc. Natl. Acad. Sci. U.S.A.* **100** (2003) p. 1690.
19. D. Fotiadis, S. Scheuring, S.A. Müller, A. Engel, and D.J. Müller, *Micron* **33** (2002) p. 385.
20. F.A. Schabert, C. Henn, and A. Engel, *Science* **268** (1995) p. 92.
21. D. Fotiadis, L. Hasler, D.J. Müller, H. Stahlberg, J. Kistler, and A. Engel, *J. Mol. Biol.* **300** (2000) p. 779.
22. D.J. Müller, G.M. Hand, A. Engel, and G.E. Sosinsky, *EMBO J.* **21** (2002) p. 3598.
23. D. Fotiadis, D.J. Müller, G. Tsiotis, L. Hasler, P. Tittman, T. Mini, P. Jenö, H. Gross, and A. Engel, *J. Mol. Biol.* **283** (1998) p. 83.
24. C.A. Siebert, P. Qian, D. Fotiadis, A. Engel, C.N. Hunter, and P.A. Bullough, *EMBO J.* **23** (2004) p. 690.
25. D. Fotiadis, P. Qian, A. Philippsen, P.A. Bullough, A. Engel, and C.N. Hunter, *J. Biol. Chem.* **279** (2004) p. 2063.
26. A.F. Oberhauser, P.K. Hansma, M. Carrion-Vazquez, and J.M. Fernandez, *Proc. Natl. Acad. Sci. U.S.A.* **98** (2001) p. 468.
27. H. Li, W.A. Linke, A.F. Oberhauser, M. Carrion-Vazquez, J.G. Kerkvliet, H. Lu, P.E. Marszalek, and J.M. Fernandez, *Nature* **418** (2002) p. 998.
28. A.F. Oberhauser, C. Badilla-Fernandez, M. Carrion-Vazquez, and J. M. Fernandez, *J. Mol. Biol.* **319** (2002) p. 433.
29. T.E. Fisher, M. Carrion-Vazquez, A.F. Oberhauser, H. Li, P.E. Marszalek, and J.M. Fernandez, *Neuron* **27** (2000) p. 435.
30. M. Carrion-Vazquez, A.F. Oberhauser, T.E. Fisher, P.E. Marszalek, H. Li, and J.M. Fernandez, *Prog. Biophys. Mol. Biol*. **74** (2000) p. 63.
31. M. Rief, M. Gautel, and H.E. Gaub, *Adv. Exp. Med. Biol.* **481** (2000) p. 129.
32. A. Minajeva, M. Kulke, J.M. Fernandez, and W.A. Linke, *Biophys. J.* **80** (2001) p. 1442.
33. P.M. Williams, S.B. Fowler, R.B. Best, J.L. Toca-Herrera, K.A. Scott, A. Steward, and J. Clarke, *Nature* **422** (2003) p. 446.
34. P.E. Marszalek, H. Lu, H. Li, M. Carrion-Vazquez, A.F. Oberhauser, K. Schulten, and J.M. Fernandez, *Nature* **402** (1999) p. 100.
35. F. Oesterhelt, D. Oesterhelt, M. Pfeiffer, A. Engel, H.E. Gaub, and D.J. Müller, *Science* **288** (2000) p. 143.

36. D.J. Müller, M. Kessler, F. Oesterhelt, C. Möller, D. Oesterhelt, and H. Gaub, *Biophys. J.* **83** (2002) p. 3578.
37. C. Möller, D. Fotiadis, K. Suda, A. Engel, M. Kessler, and D.J. Müller, *J. Struct. Biol.* **142** (2003) p. 369.
38. H. Janovjak, M. Kessler, D. Oesterhelt, H. Gaub, and D.J. Müller, *EMBO J.* **22** (2003) p. 5220.
39. T. Ando, N. Kodera, E. Takai, D. Maruyama, K. Saito, and A. Toda, *Proc. Natl. Acad. Sci. U.S.A.* **98** (2001) p. 12468.
40. D.A. Walters, J.P. Cleveland, N.H. Thomson, P.K. Hansma, M.A. Wendman, G. Gurley, and V. Elings, *Rev. Sci. Instrum.* **67** (1996) p. 3583.
41. M.B. Viani, T.E. Schäfer, A. Chand, M. Rief, H. Gaub, and P.K. Hansma, *J. Appl. Phys.* **86** (1999) p. 2258.
42. J.L. Yang, M. Despont, B.W. Hoogenboom, U. Dreschler, P.L.T.M. Frederix, S. Martin, H.J. Hug, P. Vettiger, and A. Engel, in *Proc. 17th IEEE Intl. Conf. on Micro Electro Mechanical Systems (MEMS 2004)* (Institute of Electrical and Electronics Engineers, Piscataway, NJ, 2004) p. 560.
43. M.B. Viani, L.I. Pietrasanta, J.B. Thompson, A. Chand, I.C. Gebeshuber, J.H. Kindt, M. Richter, H.G. Hansma, and P.K. Hansma, *Nat. Struct. Biol.* **7** (2000) p. 644.
44. B.W. Hoogenboom, P.L.T.M. Frederix, S. Martin, A. Engel, and H.J. Hug (2004) in preparation.
45. P.L.T.M. Frederix, T. Akiyama, U. Staufer, C. Gerber, D. Fotiadis, D.J. Müller, and A. Engel, *Curr. Opin. Chem. Biol.* **7** (2003) p. 641.
46. T. Akiyama, M.R. Gullo, N.F. de Rooij, U. Staufer, A. Tonin, A. Engel, and P.L.T.M. Frederix, in *Proc. 12th Intl. Conf. on Scanning Tunneling Microscopy/Spectroscopy and Related Techniques*, Vol. 696, edited by P.M. Koenraad and M. Kemerink (American Institute of Physics, Eindhoven, 2003) p. 166.
47. G. Schurmann, W. Noell, U. Staufer, and N.F. de Rooij, *Ultramicroscopy* **82** (2000) p. 33.
48. M. Stopka, D. Drews, K. Mayr, M. Lacher, W. Ehrfeld, T. Kalkbrenner, M. Graf, V. Sandoghdar, and J. Mlynek, *Microelectron. Eng.* **53** (2000) p. 183.
49. A. Meister, S. Jeney, M. Liley, T. Akiyama, U. Staufer, N.F. de Rooij, and H. Heinzelmann, *Microelectron. Eng.* **67-68** (2003) p. 2003.
50. P.K. Hansma, B. Drake, O. Marti, S.A.C. Gould, and C.B. Prater, *Science* **243** (1989) p. 641. □